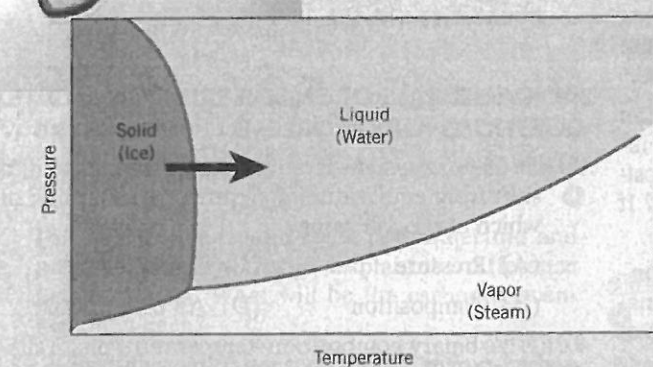
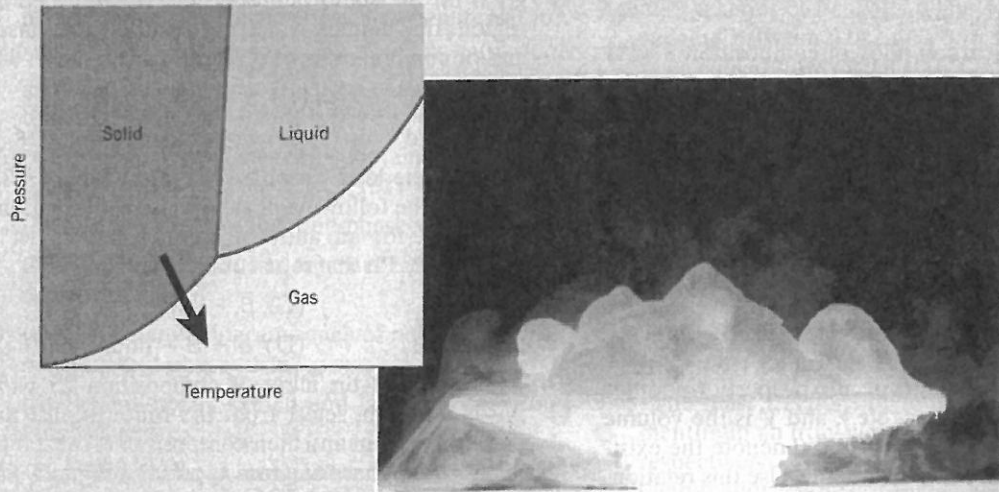


# Chapter 10 Phase Transformations: Development of Microstructure and Alteration of Mechanical Properties

SuperStock



Two pressure-temperature phase diagrams are shown: for  $\text{H}_2\text{O}$  (top) and  $\text{CO}_2$  (bottom). Phase transformations occur when phase boundaries (the red curves) on these plots are crossed as temperature and/or pressure is changed. For example, ice melts (transforms to liquid water) upon heating, which corresponds to crossing the solid-liquid phase boundary, as represented by the arrow on the  $\text{H}_2\text{O}$  phase diagram. Similarly, upon passing across the solid-gas phase boundary of the  $\text{CO}_2$  phase diagram, dry ice (solid  $\text{CO}_2$ ) sublimes (transforms into gaseous  $\text{CO}_2$ ). Again, an arrow delineates this phase transformation.



Charles D. Winters/Photo Researchers, Inc.

## WHY STUDY Phase Transformations?

The development of a set of desirable mechanical characteristics for a material often results from a phase transformation that is wrought by a heat treatment. The time and temperature dependencies of some phase transformations are conveniently represented on modified phase diagrams. It is important to know how to use these diagrams in order to design a heat

treatment for some alloy that will yield the desired room-temperature mechanical properties. For example, the tensile strength of an iron–carbon alloy of eutectoid composition (0.76 wt% C) can be varied between approximately 700 MPa (100,000 psi) and 2000 MPa (300,000 psi) depending on the heat treatment employed.

### Learning Objectives

After studying this chapter, you should be able to do the following:

1. Make a schematic fraction transformation-versus-logarithm of time plot for a typical solid-solid transformation; cite the equation that describes this behavior.
2. Briefly describe the microstructure for each of the following microconstituents that are found in steel alloys: fine pearlite, coarse pearlite, spheroidite, bainite, martensite, and tempered martensite.
3. Cite the general mechanical characteristics for each of the following microconstituents: fine pearlite, coarse pearlite, spheroidite, bainite, martensite, and tempered martensite; briefly explain these behaviors in terms of microstructure (or crystal structure).
4. Given the isothermal transformation (or continuous-cooling transformation) diagram for some iron–carbon alloy, design a heat treatment that will produce a specified microstructure.

## 10.1 INTRODUCTION

One reason metallic materials are so versatile is that their mechanical properties (strength, hardness, ductility, etc.) are subject to control and management over relatively large ranges. Three strengthening mechanisms were discussed in Chapter 7—namely grain size refinement, solid-solution strengthening, and strain hardening. Additional techniques are available in which the mechanical behavior of a metal alloy is influenced by its microstructure.

The development of microstructure in both single- and two-phase alloys typically involves some type of phase transformation—an alteration in the number and/or character of the phases. The first portion of this chapter is devoted to a brief discussion of some of the basic principles relating to transformations involving solid phases. Because most phase transformations do not occur instantaneously, consideration is given to the dependence of reaction progress on time, or the **transformation rate**. This is followed by a discussion of the development of two-phase microstructures for iron–carbon alloys. Modified phase diagrams are introduced that permit determination of the microstructure that results from a specific heat treatment. Finally, other microconstituents in addition to pearlite are presented and, for each, the mechanical properties are discussed.

transformation rate

## Phase Transformations

### 10.2 BASIC CONCEPTS

phase transformation

A variety of phase transformations are important in the processing of materials, and usually they involve some alteration of the microstructure. For purposes of this discussion, these transformations are divided into three classifications. In one group are

sum of both terms (Figure 10.2b) first increases, passes through a maximum, and finally decreases. In a physical sense, this means that as a solid particle begins to form as atoms in the liquid cluster together, its free energy first increases. If this cluster reaches a size corresponding to the critical radius  $r^*$ , then growth will continue with the accompaniment of a decrease in free energy. However, a cluster of radius less than the critical value will shrink and redissolve. This subcritical particle is an *embryo*, and the particle of radius greater than  $r^*$  is termed a *nucleus*. A critical free energy,  $\Delta G^*$ , occurs at the critical radius and, consequently, at the maximum of the curve in Figure 10.2b. This  $\Delta G^*$  corresponds to an *activation free energy*, which is the free energy required for the formation of a stable nucleus. Equivalently, it may be considered an energy barrier to the nucleation process.

Because  $r^*$  and  $\Delta G^*$  appear at the maximum on the free energy-versus-radius curve of Figure 10.2b, derivation of expressions for these two parameters is a simple matter. For  $r^*$ , we differentiate the  $\Delta G$  equation (Equation 10.1) with respect to  $r$ , set the resulting expression equal to zero, and then solve for  $r$  ( $= r^*$ ). That is,

$$\frac{d(\Delta G)}{dr} = \frac{4}{3}\pi \Delta G_v(3r^2) + 4\pi\gamma(2r) = 0 \quad (10.2)$$

which leads to the result

For homogeneous nucleation, critical radius of a stable solid particle nucleus

For homogeneous nucleation, activation free energy required for the formation of a stable nucleus

Dependence of critical radius on surface free energy, latent heat of fusion, melting temperature, and transformation temperature

Activation free energy expression

$$r^* = -\frac{2\gamma}{\Delta G_v} \quad (10.3)$$

Now, substitution of this expression for  $r^*$  into Equation 10.1 yields the following expression for  $\Delta G^*$ :

$$\Delta G^* = \frac{16\pi\gamma^3}{3(\Delta G_v)^2} \quad (10.4)$$

This volume free energy change  $\Delta G_v$  is the driving force for the solidification transformation, and its magnitude is a function of temperature. At the equilibrium solidification temperature  $T_m$ , the value of  $\Delta G_v$  is zero, and with decreasing temperature its value becomes increasingly more negative.

It can be shown that  $\Delta G_v$  is a function of temperature as

$$\Delta G_v = \frac{\Delta H_f(T_m - T)}{T_m} \quad (10.5)$$

where  $\Delta H_f$  is the latent heat of fusion (i.e., the heat given up during solidification), and  $T_m$  and the temperature  $T$  are in Kelvin. Substitution of this expression for  $\Delta G_v$  into Equations 10.3 and 10.4 yields

$$r^* = \left(-\frac{2\gamma T_m}{\Delta H_f}\right) \left(\frac{1}{T_m - T}\right) \quad (10.6)$$

and

$$\Delta G^* = \left(\frac{16\pi\gamma^3 T_m^2}{3\Delta H_f^2}\right) \frac{1}{(T_m - T)^2} \quad (10.7)$$

Thus, from these two equations, both the critical radius  $r^*$  and the activation free energy  $\Delta G^*$  decrease as temperature  $T$  decreases. (The  $\gamma$  and  $\Delta H_f$  parameters in these

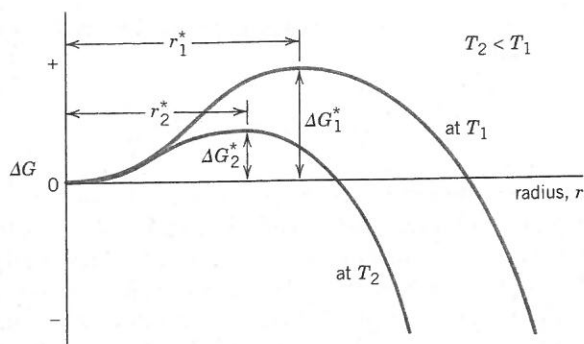


**Figure 10.3** Schematic free energy-versus-embryo/nucleus-radius curves for two different temperatures. The critical free energy change ( $\Delta G^*$ ) and critical nucleus radius ( $r^*$ ) are indicated for each temperature.

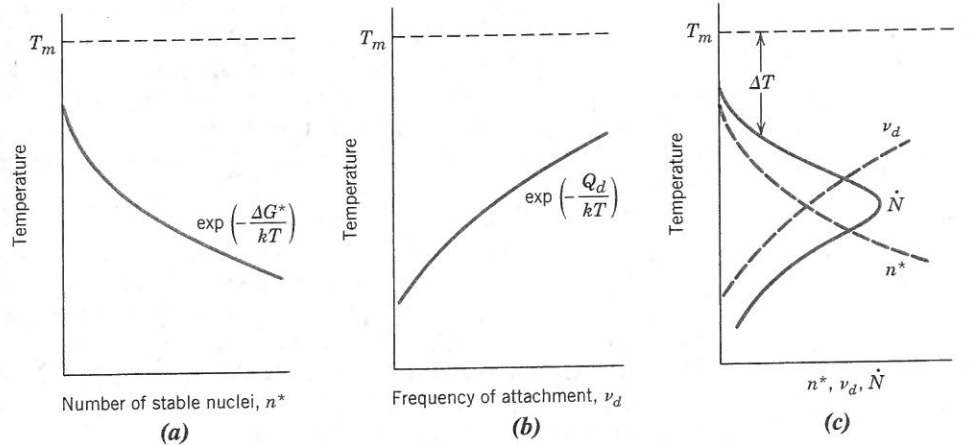
expressions are relatively insensitive to temperature changes.) Figure 10.3, a schematic  $\Delta G$ -versus- $r$  plot that shows curves for two different temperatures, illustrates these relationships. Physically, this means that with a lowering of temperature at temperatures below the equilibrium solidification temperature ( $T_m$ ), nucleation occurs more readily. Furthermore, the number of stable nuclei  $n^*$  (having radii greater than  $r^*$ ) is a function of temperature as

$$n^* = K_1 \exp\left(-\frac{\Delta G^*}{kT}\right) \quad (10.8)$$

where the constant  $K_1$  is related to the total number of nuclei of the solid phase. For the exponential term of this expression, changes in temperature have a greater effect on the magnitude of the  $\Delta G^*$  term in the numerator than the  $T$  term in the denominator. Consequently, as the temperature is lowered below  $T_m$ , the exponential term in Equation 10.8 also decreases, so that the magnitude of  $n^*$  increases. This temperature dependence ( $n^*$  versus  $T$ ) is represented in the schematic plot of Figure 10.4a.

Another important temperature-dependent step is involved in and also influences nucleation: the clustering of atoms by short-range diffusion during the formation of nuclei. The influence of temperature on the rate of diffusion (i.e., magnitude of the diffusion coefficient,  $D$ ) is given in Equation 5.8. Furthermore, this diffusion effect is related to the frequency at which atoms from the liquid attach themselves to the

**figure 10.4** For solidification, schematic plots of (a) number of stable nuclei versus temperature, (b) frequency of atomic attachment versus temperature, and (c) nucleation rate versus temperature (the dashed curves are reproduced from parts a and b).



solid nucleus,  $v_d$ . The dependence of  $v_d$  on temperature is the same as for the diffusion coefficient—namely,

$$v_d = K_2 \exp\left(-\frac{Q_d}{kT}\right) \quad (10.9)$$

where  $Q_d$  is a temperature-independent parameter—the activation energy for diffusion—and  $K_2$  is a temperature-independent constant. Thus, from Equation 10.9, a decrease of temperature results in a reduction in  $v_d$ . This effect, represented by the curve shown in Figure 10.4b, is just the reverse of that for  $n^*$  as discussed earlier.

The principles and concepts just developed are now extended to a discussion of another important nucleation parameter, the nucleation rate  $\dot{N}$  (which has units of nuclei per unit volume per second). This rate is simply proportional to the product of  $n^*$  (Equation 10.8) and  $v_d$  (Equation 10.9)—that is,

Nucleation rate expression for homogeneous nucleation

$$\dot{N} = K_3 n^* v_d = K_1 K_2 K_3 \left[ \exp\left(-\frac{\Delta G^*}{kT}\right) \exp\left(-\frac{Q_d}{kT}\right) \right]. \quad (10.10)$$

Here,  $K_3$  is the number of atoms on a nucleus surface. Figure 10.4c schematically plots nucleation rate as a function of temperature and, in addition, the curves of Figures 10.4a and 10.4b from which the  $\dot{N}$  curve is derived. Figure 10.4c shows that, with a reduction of temperature from below  $T_m$ , the nucleation rate first increases, achieves a maximum, and subsequently diminishes.

The shape of this  $\dot{N}$  curve is explained as follows: for the upper region of the curve (a sudden and dramatic increase in  $\dot{N}$  with decreasing  $T$ ),  $\Delta G^*$  is greater than  $Q_d$ , which means that the  $\exp(-\Delta G^*/kT)$  term of Equation 10.10 is much smaller than  $\exp(-Q_d/kT)$ . In other words, the nucleation rate is suppressed at high temperatures because of a small activation driving force. With continued reduction of temperature, there comes a point at which  $\Delta G^*$  becomes smaller than the temperature-independent  $Q_d$ , with the result that  $\exp(-Q_d/kT) < \exp(-\Delta G^*/kT)$ , or that, at lower temperatures, a low atomic mobility suppresses the nucleation rate. This accounts for the shape of the lower curve segment (a precipitous reduction of  $\dot{N}$  with a continued reduction of temperature). Furthermore, the  $\dot{N}$  curve of Figure 10.4c necessarily passes through a maximum over the intermediate temperature range, where values for  $\Delta G^*$  and  $Q_d$  are of approximately the same magnitude.

Several qualifying comments are in order regarding the preceding discussion. First, although we assumed a spherical shape for nuclei, this method may be applied to any shape with the same final result. Furthermore, this treatment may be used for types of transformations other than solidification (i.e., liquid–solid)—for example, solid–vapor and solid–solid. However, magnitudes of  $\Delta G_v$  and  $\gamma$ , in addition to diffusion rates of the atomic species, will undoubtedly differ among the various transformation types. In addition, for solid–solid transformations, there may be volume changes attendant to the formation of new phases. These changes may lead to the introduction of microscopic strains, which must be taken into account in the  $\Delta G$  expression of Equation 10.1 and, consequently, will affect the magnitudes of  $r^*$  and  $\Delta G^*$ .

From Figure 10.4c it is apparent that during the cooling of a liquid, an appreciable nucleation rate (i.e., solidification) will begin only after the temperature has been lowered to below the equilibrium solidification (or melting) temperature ( $T_m$ ). This phenomenon is termed *supercooling* (or *undercooling*), and the degree of supercooling for homogeneous nucleation may be significant (on the order of several hundred degrees Kelvin) for some systems. Table 10.1 shows, for several materials, typical degrees of supercooling for homogeneous nucleation.

**Table 10.1**

Degree of Supercooling ( $\Delta T$ ) Values (Homogeneous Nucleation) for Several Metals

Metal	$\Delta T$ (°C)
Antimony	135
Germanium	227
Silver	227
Gold	230
Copper	236
Iron	295
Nickel	319
Cobalt	330
Palladium	332

Source: D. Turnbull and R. E. Cech, "Microscopic Observation of the Solidification of Small Metal Droplets," *J. Appl. Phys.*, **21**, 808 (1950).

### EXAMPLE PROBLEM 10.1

#### Computation of Critical Nucleus Radius and Activation Free Energy

- For the solidification of pure gold, calculate the critical radius  $r^*$  and the activation free energy  $\Delta G^*$  if nucleation is homogeneous. Values for the latent heat of fusion and surface free energy are  $-1.16 \times 10^9 \text{ J/m}^3$  and  $0.132 \text{ J/m}^2$ , respectively. Use the supercooling value in Table 10.1.
- Now, calculate the number of atoms found in a nucleus of critical size. Assume a lattice parameter of  $0.413 \text{ nm}$  for solid gold at its melting temperature.

#### Solution

- In order to compute the critical radius, we employ Equation 10.6, using the melting temperature of  $1064^\circ\text{C}$  for gold, assuming a supercooling value of  $230^\circ\text{C}$  (Table 10.1), and realizing that  $\Delta H_f$  is negative. Hence

$$\begin{aligned} r^* &= \left( -\frac{2\gamma T_m}{\Delta H_f} \right) \left( \frac{1}{T_m - T} \right) \\ &= \left[ -\frac{(2)(0.132 \text{ J/m}^2)(1064 + 273 \text{ K})}{-1.16 \times 10^9 \text{ J/m}^3} \right] \left( \frac{1}{230 \text{ K}} \right) \\ &= 1.32 \times 10^{-9} \text{ m} = 1.32 \text{ nm} \end{aligned}$$

For computation of the activation free energy, Equation 10.7 is employed. Thus,

$$\begin{aligned} \Delta G^* &= \left( \frac{16\pi\gamma^3 T_m^2}{3\Delta H_f^2} \right) \frac{1}{(T_m - T)^2} \\ &= \left[ \frac{(16)(\pi)(0.132 \text{ J/m}^2)^3 (1064 + 273 \text{ K})^2}{(3)(-1.16 \times 10^9 \text{ J/m}^3)^2} \right] \left[ \frac{1}{(230 \text{ K})^2} \right] \\ &= 9.64 \times 10^{-19} \text{ J} \end{aligned}$$

- In order to compute the number of atoms in a nucleus of critical size (assuming a spherical nucleus of radius  $r^*$ ), it is first necessary to determine the number of unit cells, which we then multiply by the number of atoms per unit cell. The number of unit cells found in this critical nucleus is just the ratio of critical nucleus and unit cell volumes. Inasmuch as gold has the FCC crystal structure (and a cubic unit cell), its unit cell volume is just  $a^3$ , where  $a$  is the lattice parameter (i.e., unit cell edge length); its value is  $0.413 \text{ nm}$ , as cited in the

problem statement. Therefore, the number of unit cells found in a radius of critical size is just

$$\begin{aligned}\# \text{ unit cells/particle} &= \frac{\text{critical nucleus volume}}{\text{unit cell volume}} = \frac{\frac{4}{3}\pi r^*{}^3}{a^3} \\ &= \frac{\left(\frac{4}{3}\right)(\pi)(1.32 \text{ nm})^3}{(0.413 \text{ nm})^3} = 137 \text{ unit cells}\end{aligned}\quad (10.11)$$

Because of the equivalence of four atoms per FCC unit cell (Section 3.4), the total number of atoms per critical nucleus is just

$$(137 \text{ unit cells/critical nucleus})(4 \text{ atoms/unit cell}) = 548 \text{ atoms/critical nucleus}$$

### Heterogeneous Nucleation

Although levels of supercooling for homogeneous nucleation may be significant (on occasion several hundred degrees Celsius), in practical situations they are often on the order of only several degrees Celsius. The reason for this is that the activation energy (i.e., energy barrier) for nucleation ( $\Delta G^*$  of Equation 10.4) is lowered when nuclei form on preexisting surfaces or interfaces, because the surface free energy ( $\gamma$  of Equation 10.4) is reduced. In other words, it is easier for nucleation to occur at surfaces and interfaces than at other sites. Again, this type of nucleation is termed *heterogeneous*.

In order to understand this phenomenon, let us consider the nucleation, on a flat surface, of a solid particle from a liquid phase. It is assumed that both the liquid and solid phases "wet" this flat surface—that is, both of these phases spread out and cover the surface; this configuration is depicted schematically in Figure 10.5. Also noted in the figure are three interfacial energies (represented as vectors) that exist at two-phase boundaries— $\gamma_{SL}$ ,  $\gamma_{SI}$ , and  $\gamma_{IL}$ —as well as the wetting angle  $\theta$  (the angle between the  $\gamma_{SI}$  and  $\gamma_{SL}$  vectors). Taking a surface tension force balance in the plane of the flat surface leads to the following expression:

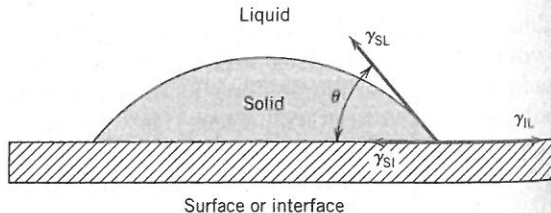
$$\gamma_{IL} = \gamma_{SI} + \gamma_{SL} \cos \theta \quad (10.12)$$

Now, using a somewhat involved procedure similar to the one presented for homogeneous nucleation (which we have chosen to omit), it is possible to derive equations for  $r^*$  and  $\Delta G^*$ ; these are as follows:

$$r^* = -\frac{2\gamma_{SL}}{\Delta G_v} \quad (10.13)$$

$$\Delta G^* = \left(\frac{16\pi\gamma_{SL}^3}{3\Delta G_v^2}\right)S(\theta) \quad (10.14)$$

**Figure 10.5** Heterogeneous nucleation of a solid from a liquid. The solid–surface ( $\gamma_{SI}$ ), solid–liquid ( $\gamma_{SL}$ ), and liquid–surface ( $\gamma_{IL}$ ), interfacial energies are represented by vectors. The wetting angle ( $\theta$ ) is also shown.



For heterogeneous nucleation of a solid particle, relationship among solid–surface, solid–liquid, and liquid–surface interfacial energies and the wetting angle

For heterogeneous nucleation, critical radius of a stable solid particle nucleus

For heterogeneous nucleation, activation free energy required for the formation of a stable nucleus

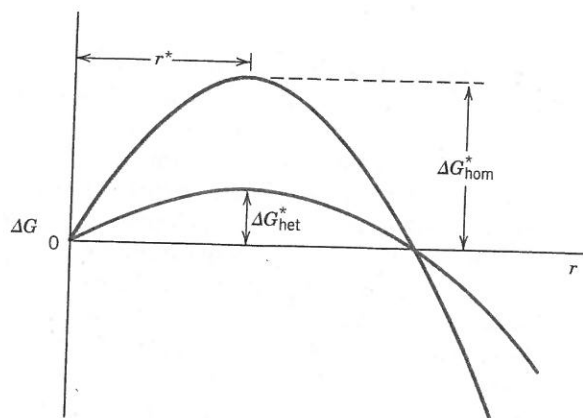


**Figure 10.6** Schematic free-energy-versus-embryo/nucleus-radius plot on which are presented curves for both homogeneous and heterogeneous nucleation. Critical free energies and the critical radius are also shown.

The  $S(\theta)$  term of this last equation is a function only of  $\theta$  (i.e., the shape of the nucleus), which has a numerical value between zero and unity.<sup>1</sup>

From Equation 10.13, it is important to note that the critical radius  $r^*$  for heterogeneous nucleation is the same as for homogeneous nucleation, inasmuch as  $\gamma_{SL}$  is the same surface energy as  $\gamma$  in Equation 10.3. It is also evident that the activation energy barrier for heterogeneous nucleation (Equation 10.14) is smaller than the homogeneous barrier (Equation 10.4) by an amount corresponding to the value of this  $S(\theta)$  function, or

$$\Delta G_{\text{het}}^* = \Delta G_{\text{hom}}^* S(\theta) \quad (10.15)$$

Figure 10.6, a schematic graph of  $\Delta G$  versus nucleus radius, plots curves for both types of nucleation and indicates the difference in the magnitudes of  $\Delta G_{\text{het}}^*$  and  $\Delta G_{\text{hom}}^*$ , in addition to the constancy of  $r^*$ . This lower  $\Delta G^*$  for heterogeneous nucleation means that a smaller energy must be overcome during the nucleation process (than for homogeneous nucleation), and, therefore, heterogeneous nucleation occurs more readily (Equation 10.10). In terms of the nucleation rate, the  $\dot{N}$ -versus- $T$  curve (Figure 10.4c) is shifted to higher temperatures for heterogeneous. This effect is represented in Figure 10.7, which also shows that a much smaller degree of supercooling ( $\Delta T$ ) is required for heterogeneous nucleation.

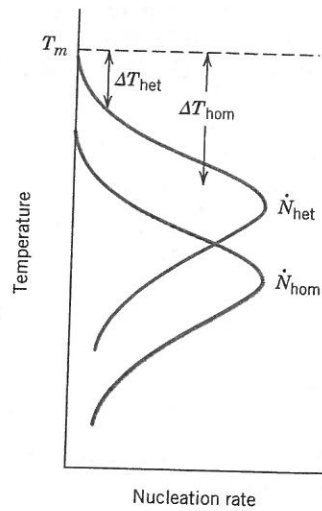


**Figure 10.7** Nucleation rate versus temperature for both homogeneous and heterogeneous nucleation. Degree of supercooling ( $\Delta T$ ) for each is also shown.

<sup>1</sup>For example, for  $\theta$  angles of  $30^\circ$  and  $90^\circ$ , values of  $S(\theta)$  are approximately 0.01 and 0.5, respectively.

### Growth

The growth step in a phase transformation begins once an embryo has exceeded the critical size,  $r^*$ , and becomes a stable nucleus. Note that nucleation will continue to occur simultaneously with growth of the new-phase particles; of course, nucleation cannot occur in regions that have already transformed into the new phase. Furthermore, the growth process will cease in any region where particles of the new phase meet because here the transformation will have reached completion.

Particle growth occurs by long-range atomic diffusion, which normally involves several steps—for example, diffusion through the parent phase, across a phase boundary, and then into the nucleus. Consequently, the growth rate  $\dot{G}$  is determined by the rate of diffusion, and its temperature dependence is the same as for the diffusion coefficient (Equation 5.8)—namely,

$$\dot{G} = C \exp\left(-\frac{Q}{kT}\right) \quad (10.16)$$

Dependence of particle growth rate on the activation energy for diffusion and temperature

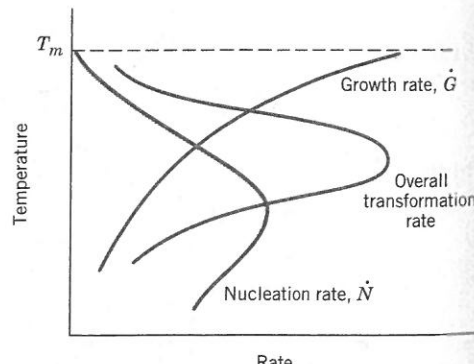
where  $Q$  (the activation energy) and  $C$  (a preexponential) are independent of temperature.<sup>2</sup> The temperature dependence of  $\dot{G}$  is represented by one of the curves in Figure 10.8; also shown is a curve for the nucleation rate,  $\dot{N}$  (again, almost always the rate for heterogeneous nucleation). Now, at a specific temperature, the overall transformation rate is equal to some product of  $\dot{N}$  and  $\dot{G}$ . The third curve of Figure 10.8, which is for the total rate, represents this combined effect. The general shape of this curve is the same as for the nucleation rate, in that it has a peak or maximum that has been shifted upward relative to the  $\dot{N}$  curve.

Whereas this treatment on transformations has been developed for solidification, the same general principles also apply to solid–solid and solid–gas transformations.

As we shall see later, the rate of transformation and the time required for the transformation to proceed to some degree of completion (e.g., time to 50% reaction completion,  $t_{0.5}$ ) are inversely proportional to one another (Equation 10.18). Thus, if the logarithm of this transformation time (i.e.,  $\log t_{0.5}$ ) is plotted versus temperature, a curve having the general shape shown in Figure 10.9b results. This “C-shaped” curve is a virtual mirror image (through a vertical plane) of the transformation rate curve of Figure 10.8, as demonstrated in Figure 10.9. The kinetics of phase transformations are often represented using logarithm time (to some degree of transformation) versus-temperature plots (for example, see Section 10.5).

Several physical phenomena may be explained in terms of the transformation rate-versus-temperature curve of Figure 10.8. First, the size of the product phase particles depends on transformation temperature. For example, for transformations that occur

**Figure 10.8** Schematic plot showing curves for nucleation rate ( $\dot{N}$ ), growth rate ( $\dot{G}$ ), and overall transformation rate versus temperature.



<sup>2</sup>Processes whose rates depend on temperature as  $\dot{G}$  in Equation 10.16 are sometimes termed **thermally activated**. Also, a rate equation of this form (i.e., having the exponential temperature dependence) is termed an **Arrhenius rate equation**.

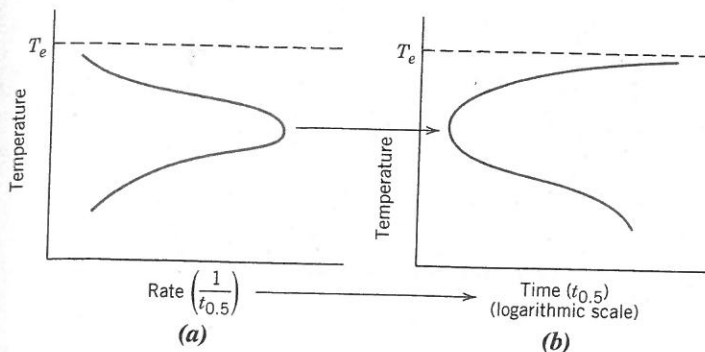


**Figure 10.9** Schematic plots of (a) transformation rate versus temperature and (b) logarithm time [to some degree (e.g., 0.5 fraction) of transformation] versus temperature. The curves in both (a) and (b) are generated from the same set of data—that is, for horizontal axes, the time [scaled logarithmically in the (b) plot] is just the reciprocal of the rate from plot (a).

at temperatures near  $T_m$ , corresponding to low nucleation and high growth rates, few nuclei form that grow rapidly. Thus, the resulting microstructure will consist of few and relatively large particles (e.g., coarse grains). Conversely, for transformations at lower temperatures, nucleation rates are high and growth rates low, which results in many small particles (e.g., fine grains).

Also, from Figure 10.8, when a material is cooled very rapidly through the temperature range encompassed by the transformation rate curve to a relatively low temperature where the rate is extremely low, it is possible to produce nonequilibrium phase structures (e.g., see Sections 10.5 and 11.9).

### Kinetic Considerations of Solid-State Transformations

kinetics

The previous discussion of this section centered on the temperature dependences of nucleation, growth, and transformation rates. The *time* dependence of rate (which is often termed the *kinetics* of a transformation) is also an important consideration, especially in the heat treatment of materials. Also, because many transformations of interest to materials scientists and engineers involve only solid phases, we devote the following discussion to the kinetics of solid-state transformations.

With many kinetic investigations, the fraction of reaction that has occurred is measured as a function of time while the temperature is maintained constant. Transformation progress is usually ascertained by either microscopic examination or measurement of some physical property (such as electrical conductivity) whose magnitude is distinctive of the new phase. Data are plotted as the fraction of transformed material versus the logarithm of time; an S-shaped curve similar to that in Figure 10.10 represents the typical kinetic behavior for most solid-state reactions. Nucleation and growth stages are also indicated in the figure.

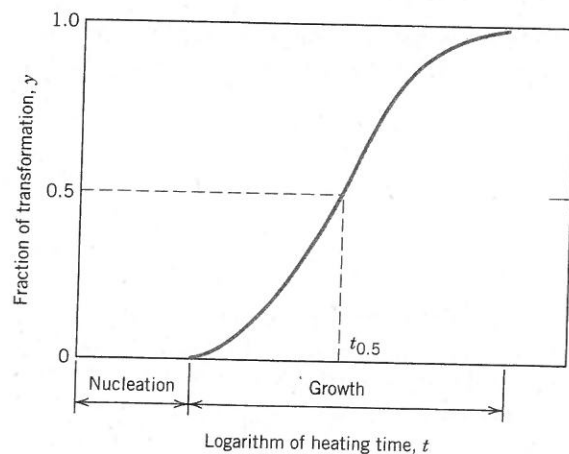


**Figure 10.10** Plot of fraction reacted versus the logarithm of time typical of many solid-state transformations in which temperature is held constant.

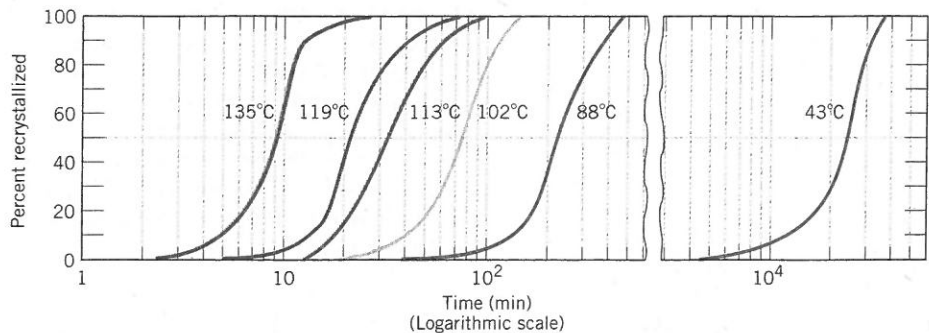


**Figure 10.11** Percent recrystallization as a function of time and at constant temperature for pure copper. (Reprinted with permission from *Metallurgical Transactions*, Vol. 188, 1950, a publication of The Metallurgical Society of AIME, Warrendale, PA. Adapted from B. F. Decker and D. Harker, "Recrystallization in Rolled Copper," *Trans. AIME*, **188**, 1950, p. 888.)

Avrami equation—  
dependence of  
fraction of  
transformation  
on time

Transformation  
rate—reciprocal  
of the halfway-to-  
completion  
transformation time

For solid-state transformations displaying the kinetic behavior in Figure 10.10, the fraction of transformation  $y$  is a function of time  $t$  as follows:

$$y = 1 - \exp(-kt^n) \quad (10.17)$$

where  $k$  and  $n$  are time-independent constants for the particular reaction. This expression is often referred to as the *Avrami equation*.

By convention, the rate of a transformation is taken as the reciprocal of time required for the transformation to proceed halfway to completion,  $t_{0.5}$ , or

$$\text{rate} = \frac{1}{t_{0.5}} \quad (10.18)$$

Temperature has a profound influence on the kinetics and thus on the rate of a transformation. This is demonstrated in Figure 10.11, which shows  $y$ -versus- $\log t$  S-shaped curves at several temperatures for the recrystallization of copper.

Section 10.5 gives a detailed discussion on the influence of both temperature and time on phase transformations.

## EXAMPLE PROBLEM 10.2

### Rate of Recrystallization Computation

It is known that the kinetics of recrystallization for some alloy obeys the Avrami equation and that the value of  $n$  is 3.1. If the fraction recrystallized is 0.30 after 20 min, determine the rate of recrystallization.

#### Solution

The rate of a reaction is defined by Equation 10.18 as

$$\text{rate} = \frac{1}{t_{0.5}}$$

Therefore, for this problem it is necessary to compute the value of  $t_{0.5}$ , the time it takes for the reaction to progress to 50% completion—or for the fraction of reaction  $y$  to equal 0.50. Furthermore, we may determine  $t_{0.5}$  using the Avrami equation, Equation 10.17:

$$y = 1 - \exp(-kt^n)$$

The problem statement provides us with the value of  $y$  (0.30) at some time  $t$  (20 min), and also the value of  $n$  (3.1) from which data it is possible to compute the value of the constant  $k$ . In order to perform this calculation, some algebraic manipulation of Equation 10.17 is necessary. First, we rearrange this expression as follows:

$$\exp(-kt^n) = 1 - y$$

Taking natural logarithms of both sides leads to

$$-kt^n = \ln(1 - y) \quad (10.17a)$$

Now, solving for  $k$ ,

$$k = -\frac{\ln(1 - y)}{t^n}$$

Incorporating values cited above for  $y$ ,  $n$ , and  $t$  yields the following value for  $k$ :

$$k = -\frac{\ln(1 - 0.30)}{(20 \text{ min})^{3.1}} = 3.30 \times 10^{-5}$$

At this point, we want to compute  $t_{0.5}$ —the value of  $t$  for  $y = 0.5$ —which means that it is necessary to establish a form of Equation 10.17 in which  $t$  is the dependent variable. This is accomplished using a rearranged form of Equation 10.17a as

$$t^n = -\frac{\ln(1 - y)}{k}$$

From which we solve for  $t$

$$t = \left[ -\frac{\ln(1 - y)}{k} \right]^{1/n}$$

And for  $t = t_{0.5}$ , this equation becomes

$$t_{0.5} = \left[ -\frac{\ln(1 - 0.5)}{k} \right]^{1/n}$$

Now, substituting into this expression the value of  $k$  determined above, as well as the value of  $n$  cited in the problem statement (viz., 3.1), we calculate  $t_{0.5}$  as follows:

$$t_{0.5} = \left[ -\frac{\ln(1 - 0.5)}{3.30 \times 10^{-5}} \right]^{1/3.1} = 24.8 \text{ min}$$

And, finally, from Equation 10.18, the rate is equal to

$$\text{rate} = \frac{1}{t_{0.5}} = \frac{1}{24.8 \text{ min}} = 4.0 \times 10^{-2} (\text{min})^{-1}$$

## 10.4 METASTABLE VERSUS EQUILIBRIUM STATES

Phase transformations may be wrought in metal alloy systems by varying temperature, composition, and the external pressure; however, temperature changes by means of heat treatments are most conveniently utilized to induce phase transformations. This corresponds to crossing a phase boundary on the composition–temperature phase diagram as an alloy of given composition is heated or cooled.

During a phase transformation, an alloy proceeds toward an equilibrium state that is characterized by the phase diagram in terms of the product phases and their compositions and relative amounts. As Section 10.3 notes, most phase transformations require some finite time to go to completion, and the speed or rate is often important in the relationship between the heat treatment and the development of microstructure. One limitation of phase diagrams is their inability to indicate the time period required for the attainment of equilibrium.

The rate of approach to equilibrium for solid systems is so slow that true equilibrium structures are rarely achieved. When phase transformations are induced by temperature changes, equilibrium conditions are maintained only if heating or cooling is carried out at extremely slow and unpractical rates. For other-than-equilibrium cooling, transformations are shifted to lower temperatures than indicated by the phase diagram; for heating, the shift is to higher temperatures. These phenomena are termed **supercooling** and **superheating**, respectively. The degree of each depends on the rate of temperature change; the more rapid the cooling or heating, the greater the supercooling or superheating. For example, for normal cooling rates, the iron–carbon eutectoid reaction is typically displaced 10°C to 20°C (18°F to 36°F) below the equilibrium transformation temperature.<sup>3</sup>

For many technologically important alloys, the preferred state or microstructure is a metastable one, intermediate between the initial and equilibrium states; on occasion, a structure far removed from the equilibrium one is desired. It thus becomes imperative to investigate the influence of time on phase transformations. This kinetic information is, in many instances, of greater value than knowledge of the final equilibrium state.

## Microstructural and Property Changes in Iron–Carbon Alloys

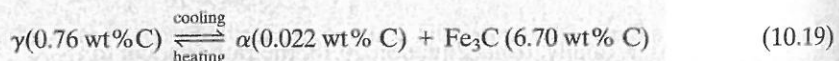
Some of the basic kinetic principles of solid-state transformations are now extended and applied specifically to iron–carbon alloys in terms of the relationships among heat treatment, the development of microstructure, and mechanical properties. This system has been chosen because it is familiar and because a wide variety of microstructures and mechanical properties is possible for iron–carbon (or steel) alloys.

### 10.5 ISOTHERMAL TRANSFORMATION DIAGRAMS

#### Pearlite

Consider again the iron–iron carbide eutectoid reaction

Eutectoid reaction  
for the iron–iron  
carbide system



which is fundamental to the development of microstructure in steel alloys. Upon cooling, austenite, having an intermediate carbon concentration, transforms into a ferrite phase, which has a much lower carbon content, and also cementite, which has a much higher carbon concentration. Pearlite is one microstructural product of this transformation (Figure 9.27); the mechanism of pearlite formation was discussed previously (Section 9.19) and demonstrated in Figure 9.28.

<sup>3</sup>It is important to note that the treatments relating to the kinetics of phase transformations in Section 10.3 are constrained to the condition of constant temperature. By way of contrast, the discussion of this section pertains to phase transformations that occur with changing temperature. This same distinction exists between Sections 10.5 (Isothermal Transformation Diagrams) and 10.6 (Continuous-Cooling Transformation Diagrams).

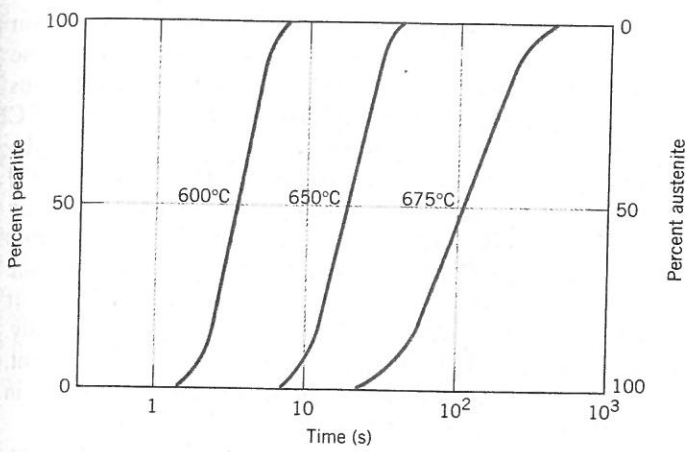


**Figure 10.12** For an iron–carbon alloy of eutectoid composition (0.76 wt% C), isothermal fraction reacted versus the logarithm of time for the austenite-to-pearlite transformation.

Temperature plays an important role in the rate of the austenite-to-pearlite transformation. The temperature dependence for an iron–carbon alloy of eutectoid composition is indicated in Figure 10.12, which plots S-shaped curves of the percentage transformation versus the logarithm of time at three different temperatures. For each curve, data were collected after rapidly cooling a specimen composed of 100% austenite to the temperature indicated; that temperature was maintained constant throughout the course of the reaction.

A more convenient way of representing both the time and temperature dependence of this transformation is shown in the bottom portion of Figure 10.13. Here, the vertical and horizontal axes are, respectively, temperature and the logarithm of time. Two solid curves are plotted; one represents the time required at each temperature

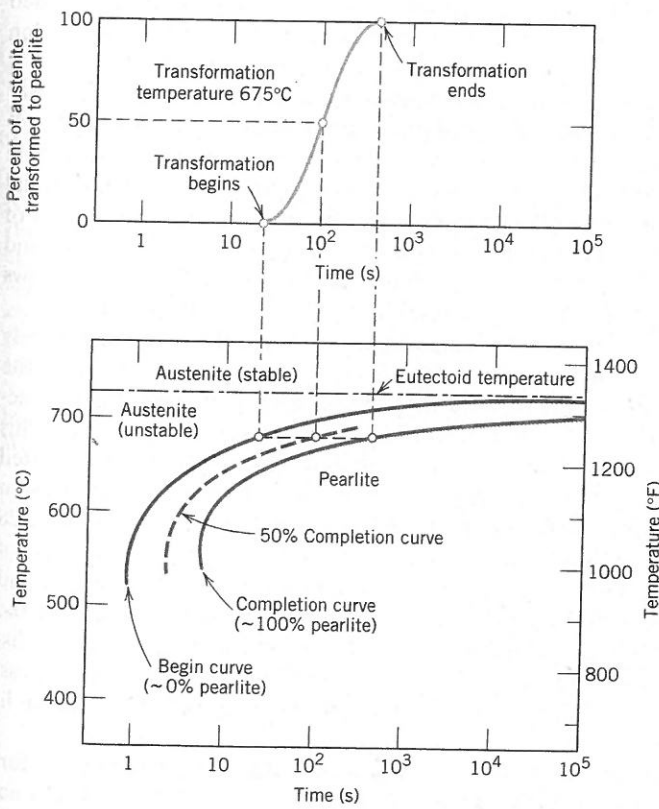


**Figure 10.13** Demonstration of how an isothermal transformation diagram (bottom) is generated from percentage transformation-versus-logarithm of time measurements (top). [Adapted from H. Boyer (Editor), *Atlas of Isothermal Transformation and Cooling Transformation Diagrams*, 1977. Reproduced by permission of ASM International, Materials Park, OH.]

for the initiation or start of the transformation, and the other is for the transformation conclusion. The dashed curve corresponds to 50% of transformation completion. These curves were generated from a series of plots of the percentage transformation versus the logarithm of time taken over a range of temperatures. The S-shape curve [for 675°C (1247°F)] in the upper portion of Figure 10.13 illustrates how the data transfer is made.

In interpreting this diagram, note first that the eutectoid temperature [727°C (1341°F)] is indicated by a horizontal line; at temperatures above the eutectoid and for all times, only austenite exists, as indicated in the figure. The austenite-to-pearlite transformation occurs only if an alloy is supercooled to below the eutectoid; as indicated by the curves, the time necessary for the transformation to begin and then end depends on temperature. The start and finish curves are nearly parallel, and they approach the eutectoid line asymptotically. To the left of the transformation start curve, only austenite (which is unstable) is present, whereas to the right of the finish curve, only pearlite exists. In between, the austenite is in the process of transforming to pearlite, and thus both microconstituents are present.

According to Equation 10.18, the transformation rate at some particular temperature is inversely proportional to the time required for the reaction to proceed to 50% completion (to the dashed line in Figure 10.13). That is, the shorter this time, the higher is the rate. Thus, from Figure 10.13, at temperatures just below the eutectoid (corresponding to just a slight degree of undercooling) very long times (on the order of  $10^5$  s) are required for the 50% transformation, and therefore the reaction rate is very slow. The transformation rate increases with decreasing temperature such that at 540°C (1000°F), only about 3 s is required for the reaction to go to 50% completion.

Several constraints are imposed on the use of diagrams like Figure 10.13. First, this particular plot is valid only for an iron–carbon alloy of eutectoid composition; for other compositions, the curves have different configurations. In addition, these plots are accurate only for transformations in which the temperature of the alloy is held constant throughout the duration of the reaction. Conditions of constant temperature are termed *isothermal*; thus, plots such as Figure 10.13 are referred to as *isothermal transformation diagrams* or sometimes as *time-temperature-transformation* (or *T-T-T*) plots.

An actual isothermal heat treatment curve (*ABCD*) is superimposed on the isothermal transformation diagram for a eutectoid iron–carbon alloy in Figure 10.14. Very rapid cooling of austenite to a given temperature is indicated by the near-vertical line *AB*, and the isothermal treatment at this temperature is represented by the horizontal segment *BCD*. Time increases from left to right along this line. The transformation of austenite to pearlite begins at the intersection, point *C* (after approximately 3.5 s), and has reached completion by about 15 s, corresponding to point *D*. Figure 10.14 also shows schematic microstructures at various times during the progression of the reaction.

The thickness ratio of the ferrite and cementite layers in pearlite is approximately 8 to 1. However, the absolute layer thickness depends on the temperature at which the isothermal transformation is allowed to occur. At temperatures just below the eutectoid, relatively thick layers of both the  $\alpha$ -ferrite and  $\text{Fe}_3\text{C}$  phases are produced; this microstructure is called **coarse pearlite**, and the region at which it forms is indicated to the right of the completion curve on Figure 10.14. At these temperatures, diffusion rates are relatively high, such that during the transformation illustrated in Figure 9.28 carbon atoms can diffuse relatively long distances, which results in the formation of thick lamellae. With decreasing temperature, the carbon diffusion rate decreases, and the layers become progressively thinner. The thin-layered structure produced in the vicinity of 540°C is termed **fine pearlite**; this is also indicated in Figure 10.14. To be discussed in Section 10.7 is the dependence of mechanical properties on lamellar thickness. Photomicrographs of coarse and fine pearlite for a eutectoid composition are shown in Figure 10.15.

For iron–carbon alloys of other compositions, a proeutectoid phase (either ferrite or cementite) coexists with pearlite, as discussed in Section 9.19. Thus, additional

isothermal  
transformation  
diagram

coarse pearlite

fine pearlite

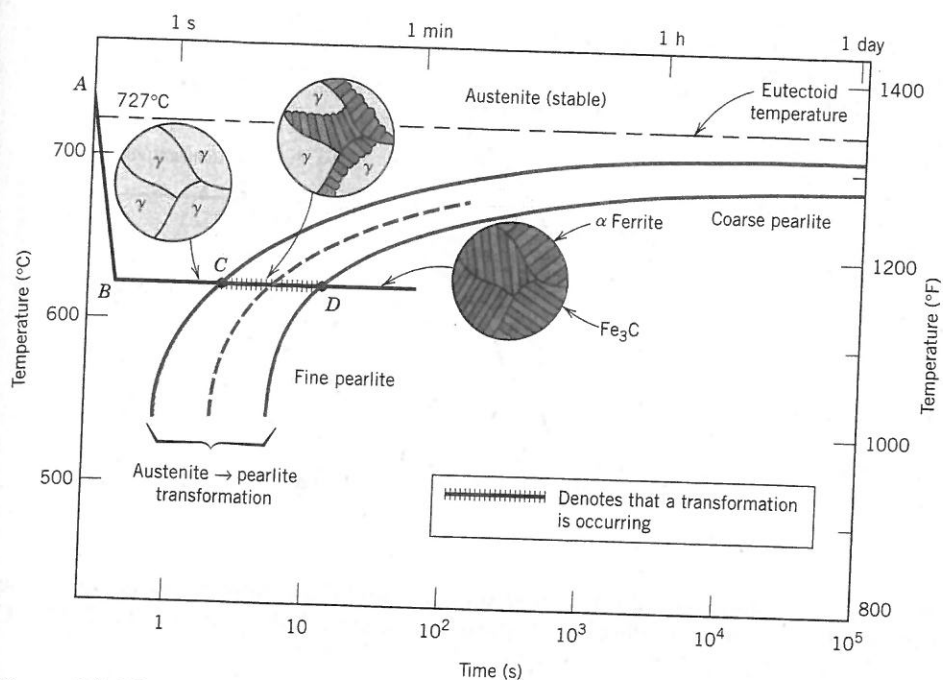


**Figure 10.14** Isothermal transformation diagram for a eutectoid iron–carbon alloy, with superimposed isothermal heat treatment curve (ABCD). Microstructures before, during, and after the austenite-to-pearlite transformation.

[Adapted from H. Boyer (Editor), *Atlas of Isothermal Transformation and Cooling Transformation Diagrams*, 1977. Reproduced by permission of ASM International, Materials Park, OH.]

**Figure 10.15**

Photomicrographs of (a) coarse pearlite and (b) fine pearlite. 3000×.

(From K. M. Ralls et al., *An Introduction to Materials Science and Engineering*, p. 361. Copyright © 1976 by John Wiley & Sons, New York. Reprinted by permission of John Wiley & Sons, Inc.)

### WileyPLUS

Tutorial Video:  
Iron–Carbon Alloy  
Microstructures

What is the  
Appearance of the  
Various Iron–Carbon  
Alloys and How Can I  
Draw Them?

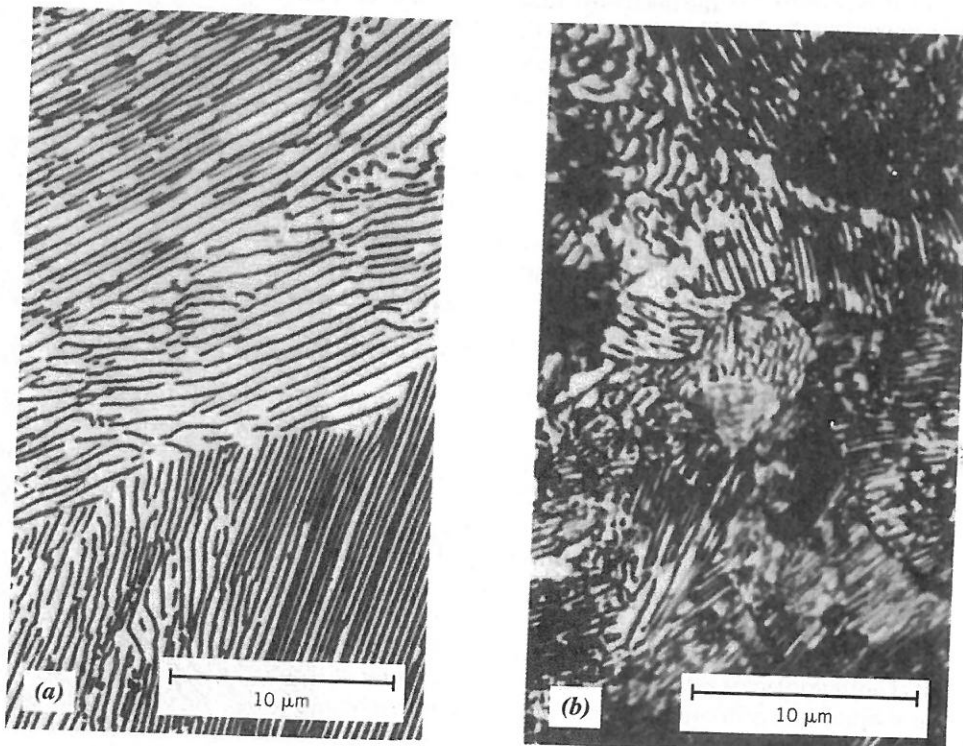
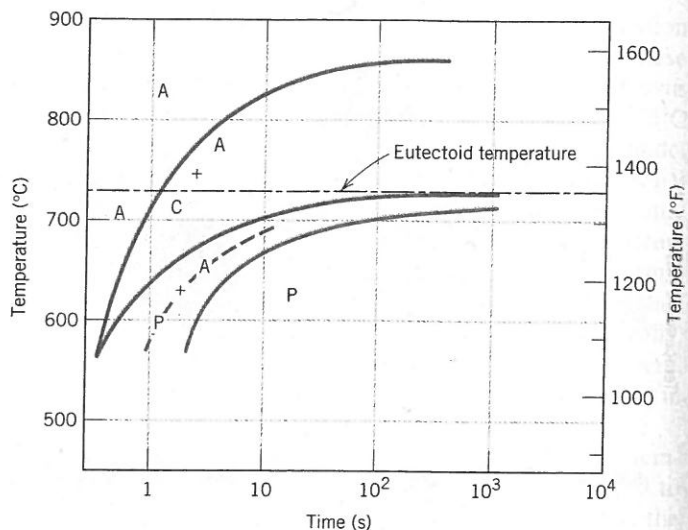


**Figure 10.16** Isothermal transformation diagram for a 1.13 wt% C iron-carbon alloy: A, austenite; C, proeutectoid cementite; P, pearlite.

[Adapted from H. Boyer (Editor), *Atlas of Isothermal Transformation and Cooling Transformation Diagrams*, 1977. Reproduced by permission of ASM International, Materials Park, OH.]



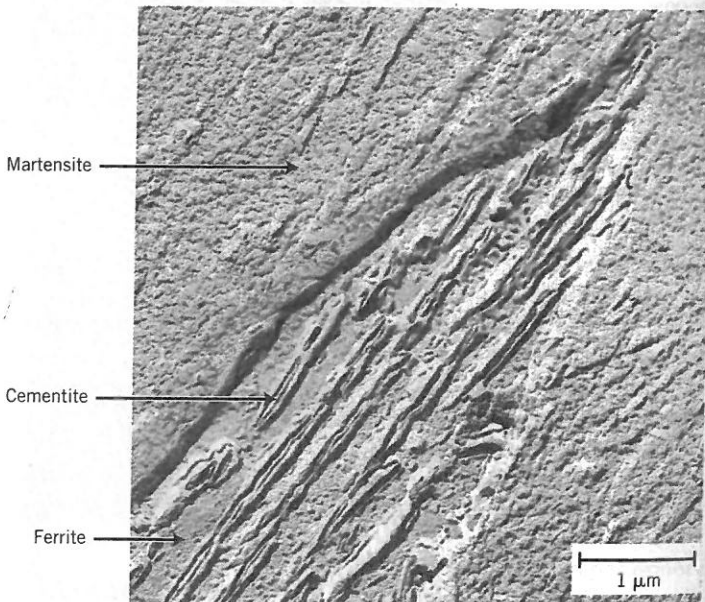
curves corresponding to a proeutectoid transformation also must be included on the isothermal transformation diagram. A portion of one such diagram for a 1.13 wt% C alloy is shown in Figure 10.16.

### Bainite

bainite

In addition to pearlite, other microconstituents that are products of the austenitic transformation exist; one of these is called **bainite**. The microstructure of bainite consists of ferrite and cementite phases, and thus diffusional processes are involved in its formation. Bainite forms as needles or plates, depending on the temperature of the transformation; the microstructural details of bainite are so fine that their resolution is possible only using electron microscopy. Figure 10.17 is an electron micrograph that shows a grain of bainite (positioned diagonally from lower left to upper right). It is composed of a ferrite matrix and elongated particles of  $\text{Fe}_3\text{C}$ ; the various phases in this micrograph have been labeled.

**Figure 10.17** Transmission electron micrograph showing the structure of bainite. A grain of bainite passes from lower left to upper right corners; it consists of elongated and needle-shape particles of  $\text{Fe}_3\text{C}$  within a ferrite matrix. The phase surrounding the bainite is martensite. (From *Metals Handbook*, Vol. 8, 8th edition, *Metallography, Structures and Phase Diagrams*, 1973. Reproduced by permission of ASM International, Materials Park, OH.)



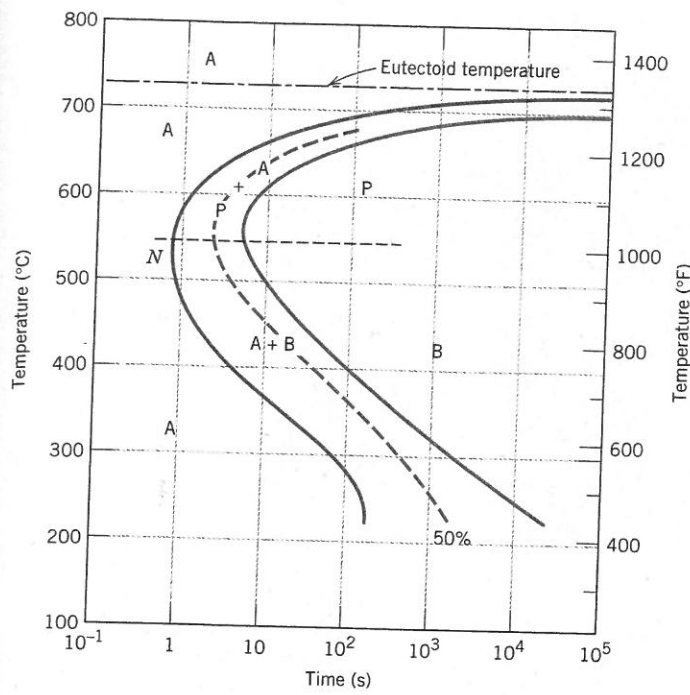


**Figure 10.18** Isothermal transformation diagram for an iron–carbon alloy of eutectoid composition, including austenite-to-pearlite (A–P) and austenite-to-bainite (A–B) transformations.

[Adapted from H. Boyer (Editor), *Atlas of Isothermal Transformation and Cooling Transformation Diagrams*, 1977. Reproduced by permission of ASM International, Materials Park, OH.]

### WileyPLUS

Tutorial Video:  
Isothermal  
Transformation  
Diagrams  
How do I Read  
a TTT Diagram?

In addition, the phase that surrounds the needle is martensite, the topic addressed by a subsequent section. Furthermore, no proeutectoid phase forms with bainite.

The time–temperature dependence of the bainite transformation may also be represented on the isothermal transformation diagram. It occurs at temperatures below those at which pearlite forms; begin-, end-, and half-reaction curves are just extensions of those for the pearlitic transformation, as shown in Figure 10.18, the isothermal transformation diagram for an iron–carbon alloy of eutectoid composition that has been extended to lower temperatures. All three curves are C-shaped and have a “nose” at point *N*, where the rate of transformation is a maximum. As may be noted, whereas pearlite forms above the nose [i.e., over the temperature range of about 540°C to 727°C (1000°F to 1341°F)], at temperatures between about 215°C and 540°C (420°F and 1000°F), bainite is the transformation product.

Note that the pearlitic and bainitic transformations are competitive with each other, and once some portion of an alloy has transformed into either pearlite or bainite, transformation to the other microconstituent is not possible without reheating to form austenite.

### Spheroidite

If a steel alloy having either pearlitic or bainitic microstructures is heated to, and left at, a temperature below the eutectoid for a sufficiently long period of time—for example, at about 700°C (1300°F) for between 18 and 24 h—yet another microstructure will form called spheroidite (Figure 10.19). Instead of the alternating ferrite and cementite lamellae (pearlite) or the microstructure observed for bainite, the Fe<sub>3</sub>C phase appears as spherelike particles embedded in a continuous  $\alpha$ -phase matrix. This transformation occurs by additional carbon diffusion with no change in the compositions or relative amounts of ferrite and cementite phases. The driving force for this transformation is the reduction in  $\alpha$ -Fe<sub>3</sub>C phase boundary area. The kinetics of spheroidite formation is not included on isothermal transformation diagrams.

spheroidite

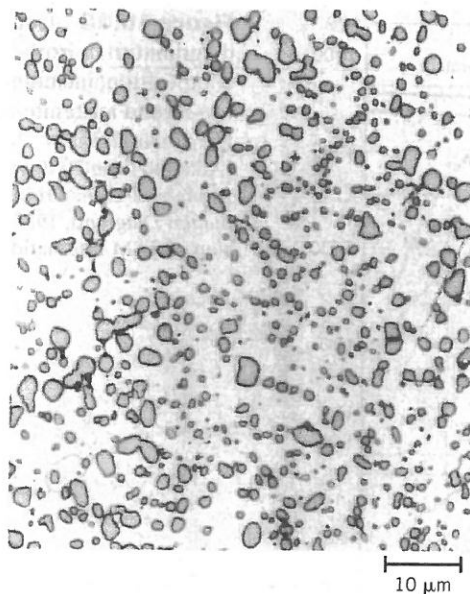


**Figure 10.19** Photomicrograph of a steel having a spheroidite microstructure. The small particles are cementite; the continuous phase is  $\alpha$ -ferrite. 1000 $\times$ . (Copyright 1971 by United States Steel Corporation.)

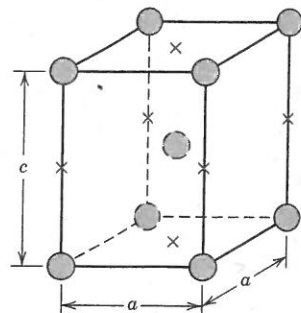


**Figure 10.20** The body-centered tetragonal unit cell for martensitic steel showing iron atoms (circles) and sites that may be occupied by carbon atoms (x's). For this tetragonal unit cell,  $c > a$ .

**Concept Check 10.1** Which is more stable, the pearlitic or the spheroiditic microstructure? Why?

[The answer may be found at [www.wiley.com/college/callister](http://www.wiley.com/college/callister) (Student Companion Site).]

### Martensite

martensite

Yet another microconstituent or phase called martensite is formed when austenitized iron–carbon alloys are rapidly cooled (or quenched) to a relatively low temperature (in the vicinity of the ambient). Martensite is a nonequilibrium single-phase structure that results from a diffusionless transformation of austenite. It may be thought of as a transformation product that is competitive with pearlite and bainite. The martensitic transformation occurs when the quenching rate is rapid enough to prevent carbon diffusion. Any diffusion whatsoever results in the formation of ferrite and cementite phases.

The martensitic transformation is not well understood. However, large numbers of atoms experience cooperative movements, in that there is only a slight displacement of each atom relative to its neighbors. This occurs in such a way that the FCC austenite experiences a polymorphic transformation to a body-centered tetragonal (BCT) martensite. A unit cell of this crystal structure (Figure 10.20) is simply a body-centered cube that has been elongated along one of its dimensions; this structure is distinctly different from that for BCC ferrite. All the carbon atoms remain as interstitial impurities in martensite; as such, they constitute a supersaturated solid solution that is capable of rapidly transforming to other structures if heated to temperatures at which diffusion rates become



**Figure 10.21** Photomicrograph showing the martensitic microstructure. The needle-shape grains are the martensite phase, and the white regions are austenite that failed to transform during the rapid quench. 1220×.

(Photomicrograph courtesy of United States Steel Corporation.)

appreciable. Many steels, however, retain their martensitic structure almost indefinitely at room temperature.

The martensitic transformation is not, however, unique to iron–carbon alloys. It is found in other systems and is characterized, in part, by the diffusionless transformation.

Because the martensitic transformation does not involve diffusion, it occurs almost instantaneously; the martensite grains nucleate and grow at a very rapid rate—the velocity of sound within the austenite matrix. Thus the martensitic transformation rate, for all practical purposes, is time independent.

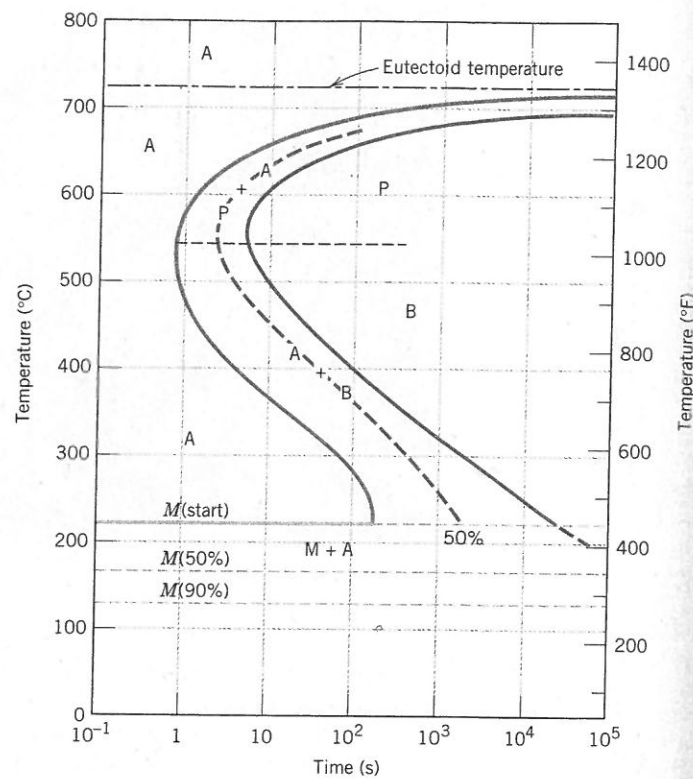
Martensite grains take on a platelike or needlelike appearance, as indicated in Figure 10.21. The white phase in the micrograph is austenite (retained austenite) that did not transform during the rapid quench. As already mentioned, martensite as well as other microconstituents (e.g., pearlite) can coexist.

Being a nonequilibrium phase, martensite does not appear on the iron–iron carbide phase diagram (Figure 9.24). The austenite-to-martensite transformation, however, is represented on the isothermal transformation diagram. Because the martensitic transformation is diffusionless and instantaneous, it is not depicted in this diagram as the pearlitic and bainitic reactions are. The beginning of this transformation is represented by a horizontal line designated  $M(\text{start})$  (Figure 10.22). Two other horizontal and dashed lines, labeled  $M(50\%)$  and  $M(90\%)$ , indicate percentages of the austenite-to-martensite transformation. The temperatures at which these lines are located vary with alloy composition, but they must be relatively low because carbon diffusion must be virtually nonexistent.<sup>4</sup> The horizontal and linear character of these lines indicates that the martensitic transformation is independent of time; it is a function only of the temperature to which the alloy is quenched or rapidly cooled. A transformation of this type is termed an **athermal transformation**.

a  
thermal  
transformation

<sup>4</sup>The alloy that is the subject of Figure 10.21 is not an iron–carbon alloy of eutectoid composition; furthermore, its 100% martensite transformation temperature lies below room temperature. Because the photomicrograph was taken at room temperature, some austenite (i.e., the retained austenite) is present, having not transformed to martensite.

**Figure 10.22** The complete isothermal transformation diagram for an iron–carbon alloy of eutectoid composition: A, austenite; B, bainite; M, martensite; P, pearlite.



Consider an alloy of eutectoid composition that is very rapidly cooled from a temperature above 727°C (1341°F) to, say, 165°C (330°F). From the isothermal transformation diagram (Figure 10.22) it may be noted that 50% of the austenite will immediately transform into martensite; as long as this temperature is maintained, there will be no further transformation.

The presence of alloying elements other than carbon (e.g., Cr, Ni, Mo, and W) may cause significant changes in the positions and shapes of the curves in the isothermal transformation diagrams. These include (1) shifting to longer times the nose of the austenite-to-pearlite transformation (and also a proeutectoid phase nose, if such exists), and (2) the formation of a separate bainite nose. These alterations may be observed by comparing Figures 10.22 and 10.23, which are isothermal transformation diagrams for carbon and alloy steels, respectively.

Steels in which carbon is the prime alloying element are termed **plain carbon steels**, whereas **alloy steels** contain appreciable concentrations of other elements, including those cited in the preceding paragraph. Section 11.2 discusses further the classification and properties of ferrous alloys.

plain carbon steel  
alloy steel

**Concept Check 10.2** Cite two major differences between martensitic and pearlitic transformations.

[The answer may be found at [www.wiley.com/college/callister](http://www.wiley.com/college/callister) (Student Companion Site).]